CARBON letters

Original Articles
Carbon Letters Vol. 28, 72-80 (2018)

Empirical relationship between band gap and synthesis parameters of chemical vapor deposition-synthesized multiwalled carbon nanotubes

Oyema E. Obasogie[1], Ambali S. Abdulkareem[1,2], Is'haq A. Mohammed[1,2,♠], Mercy T. Bankole[2,3], Jimoh. O. Tijani[2,3], and Oladiran K. Abubakre[2,4]

[1]Chemical Engineering Department, Federal University of Technology, Minna, Nigeria
[2]Nanotechnology Group, Centre for Genetic Engineering and Biotechnology (CGEB), Federal University of Technology, Minna, Nigeria
[3]Chemistry Department, School of Pure Sciences, Federal University of Technology, Minna, Nigeria
[4]Mechanical Engineering Department, Federal University of Technology, Minna, Nigeria

Article Info
Received 13 February 2018
Accepted 20 March 2018

♠Corresponding Author
E-mail: ichemsoft@gmail.com
Tel: +234-8060134955-

Open Access
DOI: http://dx.doi.org/10.5714/CL.2018.28.072

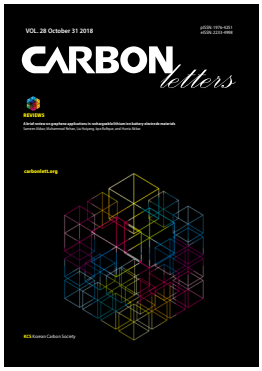

http://carbonlett.org

pISSN: 1976-4251
eISSN: 2233-4998

Abstract

In this study, an empirical relationship between the energy band gap of multi-walled carbon nanotubes (MWCNTs) and synthesis parameters in a chemical vapor deposition (CVD) reactor using factorial design of experiment was established. A bimetallic (Fe-Ni) catalyst supported on $CaCO_3$ was synthesized via wet impregnation technique and used for MWCNT growth. The effects of synthesis parameters such as temperature, time, acetylene flow rate, and argon carrier gas flow rate on the MWCNTs energy gap, yield, and aspect ratio were investigated. The as-prepared supported bimetallic catalyst and the MWCNTs were characterized for their morphologies, microstructures, elemental composition, thermal profiles and surface areas by high-resolution scanning electron microscope, high resolution transmission electron microscope, energy dispersive X-ray spectroscopy, thermal gravimetry analysis and Brunauer-Emmett-Teller. A regression model was developed to establish the relationship between band gap energy, MWCNTs yield and aspect ratio. The results revealed that the optimum conditions to obtain high yield and quality MWCNTs of 159.9% were: temperature (700ºC), time (55 min), argon flow rate (230.37 mL min^{-1}) and acetylene flow rate (150 mL min^{-1}) respectively. The developed regression models demonstrated that the estimated values for the three response variables; energy gap, yield and aspect ratio, were 0.246 eV, 557.64 and 0.82. The regression models showed that the energy band gap, yield, and aspect ratio of the MWCNTs were largely influenced by the synthesis parameters and can be controlled in a CVD reactor.

Key words: multi-walled carbon nanotubes, factorial design, energy gap, regression model, scanning electron microscopy, transmission electron microscope, chemical vapor deposition

1. Introduction

Researchers have extensively explored different synthesis protocols to produce large quantities of high quality carbon nanotubes (CNTs), which exhibit exceptional mechanical, chemical, and electronic properties [1]. Such unique characteristics, including high tensile strength, high elastic modulus, high thermal conductivity, and tendencies to withstand high current densities, make the CNTs suitable for different applications in electronics and materials science. In particular, single-walled carbon nanotubes (SWCNTs), and multi-walled carbon nanotubes (MWCNTs) are growing in popularity for applications in new electronic devices [2].

The nanotubes have been synthesized by several methods, including arc discharge, laser ablation, electrolysis, sonochemical (or hydrothermal) and various forms of chemical vapor deposition (CVD) methods [1,3]. Among these, the catalytic chemical vapor deposition (CCVD) method remains the most popular. CCVD is a simple and economically viable technique for preparing high-quality and high-quantity CNTs in continuous mode, and at a significantly lower temperature than other techniques [4]. In a typical CCVD method, MWCNTs are obtained via deposition of acetylene or methane gas onto supported single- or combined transition metal catalysts (such as Fe, Co, Ni, Fe-Co, Fe-Ni, or Fe-Ni-Co on $CaCO_3$), which are placed inside a long horizontal furnace [3,5-8]. The advantages offered by bimetallic catalysts, and by $CaCO_3$ as catalyst support for CNTs synthesis, have been well-reported in the literature [4].

Despite advances in the MWCNTs synthesis techniques, up to commercial scale production, investigations of controlled synthesis methods to obtain tailored nanotube properties for specific applications are continuing [9]. For instance, the use of MW*CNTs* in sensor devices is one of their most promising *applications* in *electronics*. *Such* sensors need to exhibit high sensitivity and selectivity, as well as fast response and recovery [10].

A number of experimental measurements are available to study the nanotubes' electronic properties [11-13], but most of the literature investigating the dependence of CNT electronic properties on their chirality has been largely based on theoretical physical principles [14-18]. In particular, first-principle calculations have been useful for predicting many of the electronic properties of CNTs. Theoretically, if the chirality and the diameter of MWCNTs can be controlled during MWCNT synthesis, then it would be possible to obtain desired properties for different electronic applications, based on the growth conditions.

One of the important electronic properties of MWCNTs is the band structure, and this has been the focus of several theoretical simulations [14-18].Depending on their chirality and diameter, MWCNTs exhibit various band gaps, which in turn determine the insulating, semiconducting, or metallic properties of the nanotubes. In addition, MWCNTs can behave as a ballistic conductor at room temperature. Ballistic electronic transport can occur in a conductor whose length is smaller than the electronic mean free path [2]. The metallic or semiconducting MWCNTs can be used as wires on circuit boards or a channel in transistors. Nonetheless, empirical relationships relating CNT synthesis conditions to the nanotubes' electronic properties have not been well-explored.

Instead of experimental measurements of MWCNTs band gaps, the present study relied on the widely used approximation based on the tight-binding model of grapheme π-bands with the nearest-neighbor [19] for semi-conducting nanotubes, as modified by Jamal and Arefin (2011). Because MWCNTs are ballistic conductors at room temperature, we approximated the band gaps of metallic MWCNTs to be three times as large as those of semiconducting nanotubes [20], using the modifications of Jamal and Arefin (2011).

This article reports a factorial design-synthesis of MWCNTs via CVD using a Fe-Ni/$CaCO_3$ catalyst, and establishes empirical equations that relate the MWCNTs' band gap, yield, and aspect ratio to the nanotubes' synthesis conditions.

2. Experimental

2.1. Materials

Iron nitrate nonahydrate, $Fe(NO_3)_3.9H_2O$; nickel nitrate hexahydrate, $Ni(NO_3)_2.6H_2O$; calcium carbonate, $CaCO_3$; sulphuric acid, H_2SO_4; nitric acid, HNO_3; and Argon and acetylene gases were of analytical grade with percentage purity in the range of 98 to 99.99%. All chemicals were used without further purification.

2.2. Synthesis of the Fe-Ni/$CaCO_3$ catalyst

Bimetallic (Fe-Ni) catalyst supported on $CaCO_3$ was prepared by the wet impregnation method. An equimolar (50:50 wt%) solution of Fe $(NO_3)_3.9H_2O$ and $Ni(NO_3)_2.6H_2O$ salts was impregnated with 6 g of $CaCO_3$ as the support material. The mixture was allowed to age for 1 h under continuous stirring. The homogenized slurry obtained was dried at 120˚C for 12 h. The resulting product was ground and calcined at 400°C for 16 h. The calcined samples were allowed to cool and then sieved through a 150 μm sieve and then kept for characterization.

2.3. Synthesis of MWCNTs

Design Expert version 7 was used for the factorial design of experiment shown in Table 1 to generate experimental runs where the influence of the following synthesis parameters on the catalyst yield were investigated, namely, acetylene flow rate, argon flow rate, reaction temperature, and time. About 1 g of the prepared bimetallic Fe-Ni/$CaCO_3$ catalyst obtained under the optimum conditions in Section 2.2 was used for each run.

The two-level factorial experimental design for the four CVD variables resulted in the generation of 16 experimental runs, presented in Table 2.

The yield of MWCNTs produced in the CVD with the Fe-Ni/$CaCO_3$ catalyst was determined after purification of all samples with H_2SO_4 and HNO_3 acids. The yields were calculated using the relationship presented in Eq. 1.

$$Yield(\%) = \frac{M_t - M_{cat}}{M_{cat}} \times 100 \quad (1)$$

where M_t is the total mass of the final catalyst and carbon products after the CVD reaction process, and M_{cat} is the initial mass of the Fe-Ni/$CaCO_3$ catalyst.

Table 1. Levels of factors considered in the experimental design.

Level	Time (min)	Temp (°C)	Argon flow rate (mL min^{-1})	Acetylene flow rate (mL min^{-1})
Lower (-)	45	700	230	150
Upper (+)	55	760	280	180

Table 2. Factorial experimental matrix for MWCNTs synthesis

Run	Time (min)	Temperature (°C)	Argon flow rate (mL min^{-1})	Acetylene flow rate (mL min^{-1})
1	45	700	230	150
2	55	700	230	150
3	45	760	230	150
4	55	760	230	150
5	45	700	280	150
6	55	700	280	150
7	45	760	280	150
8	55	760	280	150
9	45	700	230	180
10	55	700	230	180
11	45	760	230	180
12	55	760	230	180
13	45	700	280	180
14	55	700	280	180
15	45	760	280	180
16	55	760	280	180

2.4. Energy gap calculation and ANOVA

The energy gaps of the MWCNTs were determined for metallic (M) type and semi-conducting (S) nanotubes using the following equations:

$$E_{g-S} = \frac{2\gamma_o a_{c-c}}{d_t} + 0.21eV \quad (2)$$

$$E_{g-M} = 3\left[\frac{2\gamma_o a_{c-c}}{d_t} + 0.21eV\right] \quad (3)$$

where $E_{g\text{-}S}$ and $E_{g\text{-}M}$ depict the energy band gap (eV), γ_o = 2.7eV (or ~3.0eV for graphite and nanotubes), $a_{c\text{-}c}$ = 0.142 nm is the nearest-neighbor carbon-carbon bond length, and d_t is the nanotube diameter in nm [20,21]. In this study, the energy gaps were estimated from the diameter of the CNTs obtained from high-resolution scanning electron microscope (HRSEM)/ transmission electron microscope (TEM) micrographs, while the values of γ_o = 3.0 eV and $a_{c\text{-}c}$ = 0.142 nm were maintained.

Single-response models were developed for the MWCNTs yield, energy gap and aspect ratio using Design Expert software. Various synthesis parameters, including time, temperature, argon flow rate, and acetylene flow rate were the independent variables, while the CNTs yield, Energy gap, and Aspect ratio were the responses. The three regression models formed the basis for multi-response optimization which was carried out in the Design Expert. Logarithmic and polynomial regression equation fittings were obtained from a Kataura plot generated by graphing energy gap (eV) against the MWCNTs diameter (nm) obtained from TEM images of the samples, for metallic (M) and semi-conducting (S) nanotubes.

2.5. Characterization of the Fe-Ni/$CaCO_3$ catalyst and MWCNTs

The as-prepared catalyst-and MWCNTs synthesized at the optimum conditions were characterized in order to determine their thermal stability, surface area, nature of functional groups, degree of crystallinity, and morphology using thermal gravimetric analysis (TGA; TGA 4000, Perkin Elmer, USA), Brunauer-Emmett-Teller (BET; NOVA 4200e, Quantachrome Instruments, USA), Fourier transform infrared (Perkin Elmer Frontier Spectrometer), X-ray diffractometer (XRD; PW 1800 diffractometer, Philips, Netherlands), high-resolution scanning electron microscope coupled with electron diffraction spectrometer (HRSEM-EDS; JEM 100S, JEOL Ltd., Japan), and high-resolution transmission electron microscope (HRTEM)/selected area electron diffraction (SAED) (Philips CM20 FEG, the Netherlands).

3. Results and Discussion

The TGA profile of the calcium carbonate support used for the bimetallic catalyst was obtained over the temperature range of 0 to 700ºC at a constant heating rate of 10 mL min^{-1} under N_2 flow, and is depicted in Fig. 1.

In Fig. 1, it can be seen that the material is thermally stable up to 616ºC and beyond this, a weight loss of 97% occurred between 616 and 700ºC. This was attributed to the decomposition of $CaCO_3$ into CaO and CO_2. This informed the choice of 700ºC for the development of the Fe-Ni/$CaCO_3$ catalyst, which was utilized in CNTs production. HRSEM was used to examine the surface morphology of the prepared bimetallic Fe-Ni/$CaCO_3$ catalyst, and the results of the micrographs at low and high magnification are presented in Fig. 2.

HRSEM images at low magnification revealed the presence of scattered agglomerated, irregular and highly porous particles, whereas at higher magnification, it was found that the spherical catalyst particles were homogeneously distributed on the substrate surface ($CaCO_3$). The uniform distribution of the catalyst particles reveals the porous nature of the support material, which is an essential requirement for a catalyst to be used in CNT syn-

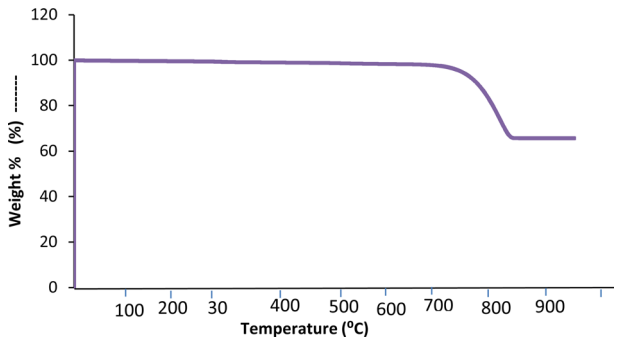

Fig. 1. Thermal profiles of $CaCO_3$ support at a heating rate of 10 mL min^{-1} under N_2.

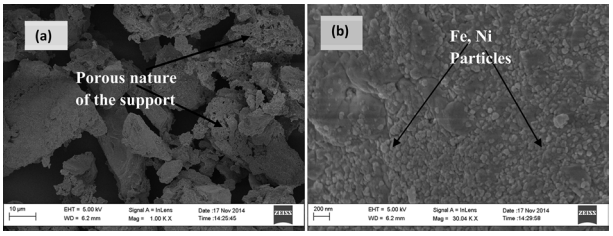

Fig. 2. HRSEM images of the Fe-Ni/$CaCO_3$ catalyst at (a) low magnification (b) high magnification.

thesis. The sizes of the Ni-Fe nanoparticles can influence the diameter of the CNTs. The HRSEM image of the catalyst presented in Fig. 2 shows that the Ni-Fe nanoparticles dispersed on the $CaCO_3$ support material are about 40 nm in size. The observed dispersion of Ni-Fe nanoparticles on the $CaCO_3$ was also supported by the accompanying EDX spectrum, showing that Ni, Fe, Ca, C and O are the dominant elements present in the sample. The corresponding EDX of the Fe-Ni/$CaCO_3$ catalyst is shown in Fig. 3.

Fig. 3 reveals the presence of the following elements: C, Ca, O, Fe, Ni, Mg and Ca in different proportions. Ca has the highest percentage of 19.26 wt% and Ni is the lowest amount. The presence of these transition elements (Fe, Ni) further confirmed the successful deposition of the catalyst particles on the support.

The EDX spectrum qualitatively confirmed the chemical components of the Ni-Fe/$CaCO_3$ catalyst. The results also showed that the nitrates in the Fe and Ni salts were converted to their respective metallic oxides during the calcination process. The EDX percentage elemental compositions of the original catalyst mixture of (C=81.66%; O=5.76%; Ca=4.21%; Fe=4.12%; Ni=4.09%; Cu=0.16) revealed that the particles contained both Fe and Ni in the ratio of 1:1 mass %, the same proportion as used in the catalyst preparation. The EDX also showed high oxygen content, which could be the result of iron and cobalt oxide formation ($NiFe_2O_4$, Fe_2O_3 and Ni_3O_4).

Also, the presence of heavy metals (Fe and Ni) around the low energy position of oxygen in the spectrum (Ring in Fig. 3) further suggests that oxygen is possibly in mixed oxides form of the following elements; Ca, Fe and Ni and hence the presence of ternary $NiFe_2O_4$ and oxides of Fe and Ni. However, the Ca, Fe, and Ni were also present individually, as found around 3.7, 6.4, and 7.5 to 8.3 keV respectively in Fig. 3.

The microstructures and the crystalline nature of the as-prepared Fe-Ni/$CaCO_3$ were examined using HRTEM. Fig. 4 show

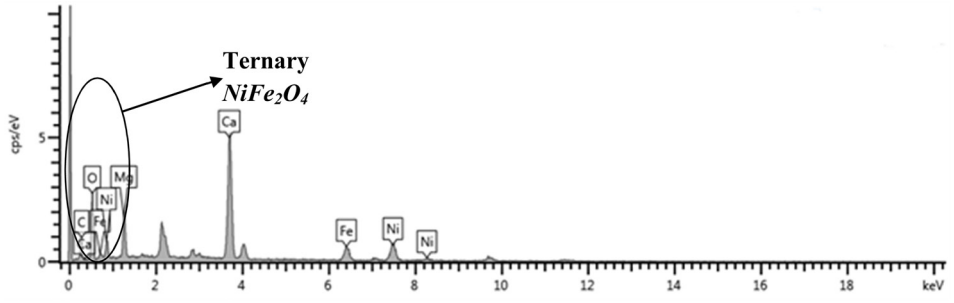

Fig. 3. EDX of Fe-Ni/$CaCO_3$ catalyst.

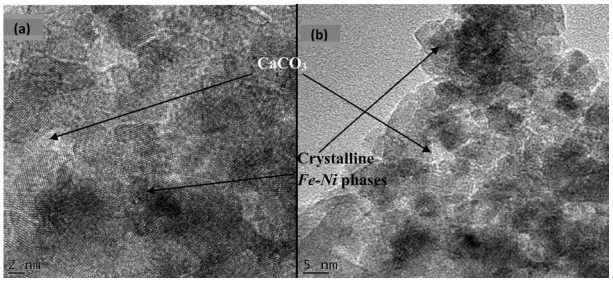

Fig. 4. HRTEM images of the Fe-Ni/$CaCO_3$ catalyst.

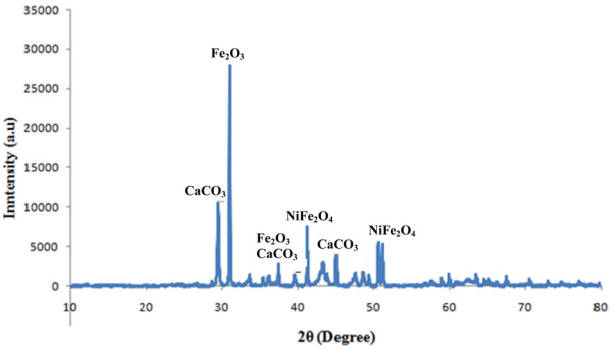

Fig. 5. XRD patterns of the Fe-Ni/$CaCO_3$ catalyst.

the presence of agglomerated iron and nickel particles effectively loaded on to the calcium carbonate. The micrographs also indicate the presence of lattice fringes which further confirmed that the prepared catalyst is highly crystalline.

As presented in Fig. 4, highly crystalline phases dispersed in the whitish $CaCO_3$ support matrix could be observed. The crystalline phase in the HRTEM suggests the possible formation of $NiFe_2O_4$ in the final catalyst. This indicates that the wet impregnation method used in the catalyst preparation was effective in dispersing the metal nanoparticles onto the support matrix. The regions of metal particles are the active part or sites of the catalyst on which the CNTs would grow, while the white bulk regions are the support-dominated regions.

Fig. 5 presents the XRD results of the Fe-Ni/$CaCO_3$ catalyst, which was used to analyze its crystalline nature. The XRD pattern reveals the presence of the following diffraction peaks at 2θ values of 29.5, 31.5, 37.8, 41.6, 43.4, 45.2 and 51.9°.

The peaks observed at Bragg angle values of 37.463, 41.1705, 44.9604, 47.1574, and 50.5629° were attributed to the existence

Table 3. Variation in MWCNTs properties with synthesis conditions in factorial design

Run	Yield (%)	TEM	Band gap (eV), S	SEM	Aspect ratio	XRD
1	101		0.2526		600	
2	181		0.2465		520	
3	34		0.2384		380	
4	81		0.2395		410	
5	93		0.2449		500	
6	127		0.2407		430	
7	67		0.2356		390	
8	80		0.2340		380	
9	184		0.2332		350	
10	198		0.2319		320	
11	100		0.2283		205	
12	72		0.2256		200	
13	179		0.2292		210	
14	162		0.2302		220	
15	93		0.2247		190	
16	91		0.2228		140	

of Fe_3C in the catalytic structure. Fe_2O_3 which was regarded as one of the resource candidates for Fe inside the catalyst was examined at Bragg angles of 33.7006° and 62.1522°. The peaks appearing at 43.1753, 57.3737, and 62.2346° could be linked to the presence of Fe_3O_4. The peaks observed at 37.3808 and 43.449° could be associated with $NiFe_2O_4$. In addition, the peak traced to a Bragg angle of 57.3737° could be that of $CaFe_2O_4$.

The surface area of the catalyst as obtained from the BET method was 63.353 m^2 g^{-1} and a pore volume of 12.9423 cm^3 g^{-1} was obtained. Overall, the properties of the Fe-Ni/$CaCO_3$ as revealed by the TGA, HRSEM, EDX, HRTEM, XRD, and BET showed its suitability for CNT growth. For the MWCNTs, which were characterized by TEM, SEM and XRD, Table 3 list the variation in MWCNTs properties with synthesis conditions in the factorial experimental design. The band gaps have been estimated from the diameters of the as-synthesized MWCNTs as obtained from TEM images.

As presented in Table 3, experimental run 10 gave the highest yield of 198% MWCNTs at conditions of 55 min, 700°C, 230 mL min^{-1} argon flowrate, and 180 mL min^{-1} acetylene flowrate. The high yield could have been favored by the combined effects of a longer reaction duration of 55 min, and higher acetylene flowrate of 180 mL min^{-1}. It can be observed from the results that the band gaps of the MWCNTs vary with the CVD synthesis parameters and other properties of the nanotubes such as yield, morphology, aspect ratio, and crystalline nature. Again, chirality and defects in nanotubes are important factors affecting their electronic properties. So, the XRD peak angles and peak shifts observed in the results (Table 3) are indicative of possible lattice distortions that could affect the energy gaps of the MWCNTs as obtained.

The results of analysis of variance (ANOVA) carried out in Design Expert software was used to generate regression models which were used for multi-response optimization. The independent variables included the various CVD parameters (time, temperature, Argon flowrate, and acetylene flowrate), and three responses (CNTs yield, energy gap, and aspect ratio) were considered. Three separate regression models were developed using ANOVA for each response (that is yield, energy gap, and aspect ratio) as presented in Tables 4-6.

The model F-value of 22.84 implies the model is significant. The factors A, B, D, AD, BC are significant model terms be-

Table 4. Response 1 (yield) ANOVA table for selected factorial model

Source	F-value	*P*-value	Remark
Model	22.84	0.0001	Significant
A (Time)	5.56	0.0461	Significant
B (Temperature)	103.03	<0.0001	Significant
C (Argon flowrate)	0.97	0.3527	Not significant
D (Acetylene flowrate)	27.75	0.0008	Significant
AD	11.98	0.0085	Significant
BC	6.04	0.0394	Significant
BD	4.51	0.0664	Significant at (P<0.1)

Table 5. Response 2 (energy gap) ANOVA table for selected factorial model

Source	F-value	*P*-value	Remark
Model	89.13	<0.0001	Significant
A (Time)	7.88	0.0205	Significant
B (Temperature)	116.24	<0.0001	Significant
C (Argon flowrate)	36.74	0.0002	Significant
D (Acetylene flowrate)	361.23	<0.0001	Significant
BD	6.36	0.0327	Significant
ABD	6.36	0.0327	Significant

Table 6. Response 3 (aspect ratio) ANOVA table for selected factorial model

Source	F-value	*P*-value	Remark
Model	76.60	<0.0001	Significant
B (Temperature)	52.46	<0.0001	Significant
C (Argon flowrate)	19.78	0.0010	significant
D (Acetylene flowrate)	226.11	<0.0001	Significant
BC	8.05	0.0161	Significant

cause they fulfill the P<0.05 criteria. An R^2 of 0.9523 was obtained, and the predicted R^2 of 0.8094 is in reasonable agreement with the adjusted R^2 of 0.9106. The source term, Argon flowrate (C) was added in the model to support hierarchy, even though it is not a significant term in the model. The overall model P-value of 0.0001 showed it is a reliable model that can be used to navigate the design space. The final regression equation in terms of coded factors is presented in Eq. 4;

$$Yield = 115.19 + 8.81A - 37.94B - 3.69C + 19.69D - 12.94AD + 9.19BC - 7.94BD \quad (4)$$

Similarly, the final Equation in terms of actual factors were:

$$Yield = -496.133 + 30.225 * Time - 1.478 * Temp - 9.09 * Argon\ Flowrate + 22.81 * Acetylene\ Flowrate - 0.173 * Time * Acetylene\ Flowrate + 0.012 * Temp * Argon\ Flowrate - 0.018 * Temp * Acetylene\ Flowrate \quad (5)$$

It was also observed that regression Eq. 4 agrees well with the behaviour of the model graphs, showing the two-way interaction effects of the synthesis conditions on the yield, as presented in Fig. 6, respectively, for acetylene flowrate and time, argon flowrate and temperature, and acetylene flowrate and temperature.

Table 5 is the ANOVA results for the Energy Gaps of the semi-conducting MWCNTs. The model F-value of 89.13 and P-value of <0.0001 implies the model is significant. Thus, the factors A, B, C, D, BD, ABD are significant model terms. An R^2 value of 0.9834 was obtained. The Predicted R^2 of 0.9477 is in reasonable agreement with the adjusted R^2 of 0.9724. The final regression equation in terms of coded factors is presented in Eq. 6:

$$Energy\ Gap = 0.23 - 9.812\times10^{-4} A - 3.76910^{-3} B - 2.119\times10^{-3} C - 6.644 \times 10^{-3} D + 8.812 \times 10^{-4} BD - 8.812 \times 10^{-4} ABD \quad (6)$$

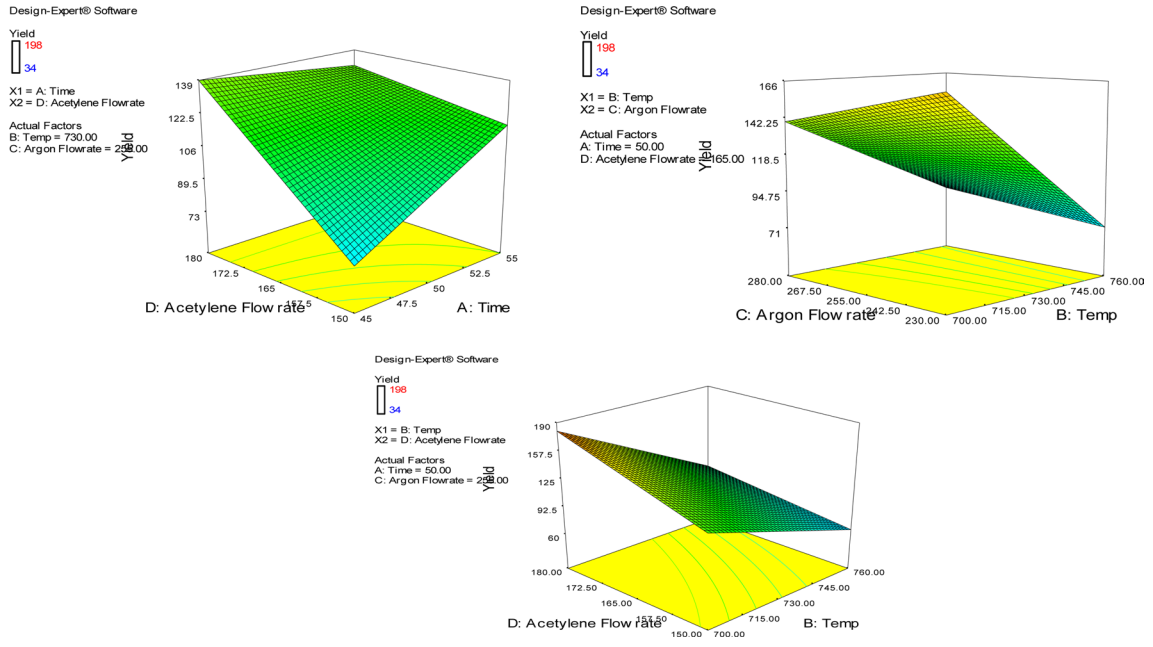

Fig. 6. Two-way interaction model graphs for yield response (a) acetylene flowrate and time; (b) argon flowrate and temperature; and (c) acetylene flowrate and temperature.

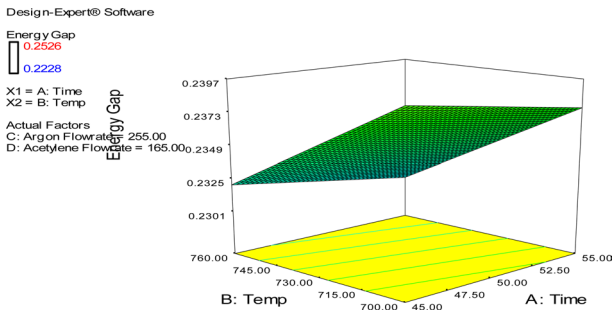

Fig. 7. Two-way interaction model graph for energy gap (temperature and time).

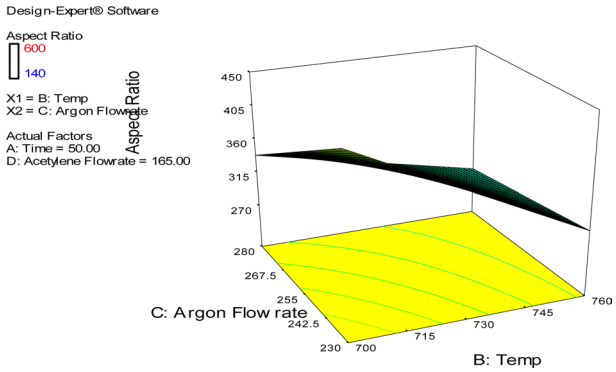

Fig. 8. Two-way interaction model graph for aspect ratio (argon flowrate and temperature).

The two-way interaction effect of temperature and time on the energy gap, which is in agreement with Eq. 6, is also supported by Fig. 7.

The model F-value of 76.60 implies the model is significant, and the factors B, C, D, BC are significant model terms fulfilling the $P<0.05$ criteria. An R^2 of 0.9653 was obtained, and the predicted R^2 of 0.9267 is in reasonable agreement with the adjusted R^2 of 0.9527. The final regression Equation in terms of coded factors is presented in Eq. 7;

$$\textit{Aspect Ratio} = 340.31 - 53.44B - 32.81C - 110.94D + 20.94BC \quad (7)$$

Again, Eq. 7 gives the final equation in terms of actual factors, which were:

$$\textit{Aspect Ratio} = 8392.31 - 8.9 * \textit{Temp} - 21.69 * \textit{Argon Flowrate} - 7.396 * \textit{Acetylene Flowrate} + 0.0279 * \textit{Temp} * \textit{Argon Flowrate} \quad (8)$$

Similar to Figs. 6 and 7, a two-way interaction effect of argon flowrate and temperature on the aspect ratio, which is in agreement with Eq. 7, is also supported by Fig. 8.

The three regression models were the basis of a multiresponse optimization that identified the combination of factors which could simulataneously predict the optimum synthesis conditions for MWCNTs' yield, Energy gap, and aspect ratio, in the case of semi-conducting nanotubes. The optimum synthesis conditions within the domain of factors selected for MWCNTs synthesis were found to be 55 min time, 700°C temperature, 230.37 mL min^{-1} Argon flowrate, and 150 mL min^{-1} acetylene flowrate. This condition achieved a simultaneous optimum, with a yield of 159.932%, Energy gap of 0.2464 eV, and Aspect ratio of 557.644, with an overall desirability of 0.820.

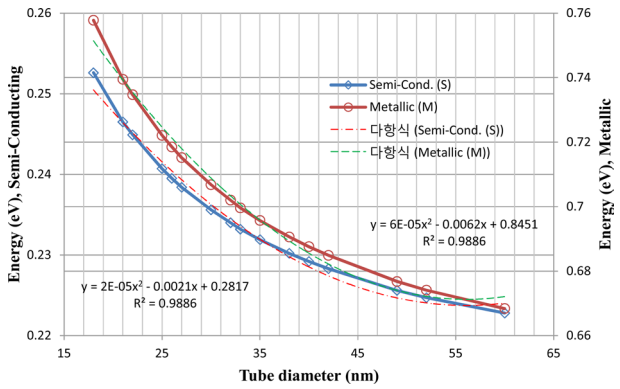

Fig. 9. Kataura plot of the synthesized MWCNTs as semi-conducting (S), and metallic (M).

Presented in Fig. 9 is a Kataura plot of band gap against nanotubes diameter (nm) obtained from TEM images of the MWCNTs samples. The Kataura plot was generated from calculated energy gaps (for semi-conducting, S, and metallic, M, nanotubes). It is a graph relating the energy of the band gaps in a CNT to its diameter.

Each MWCNT of a certain diameter can be metallic (M) or semiconducting (S); it can have several band gaps, conventionally labeled as S_{11}, S_{22}, M_{11}, M_{22}, and so on. This property results in multiple branches in the Kataura plot [22]. Both semi-conducting and metallic curves in the Kataura plot gave R^2 values of 0.969 in logarithmic regression equation fitting, and 0.988 in two-degree polynomial regression equation fitting, as presented in Eqs. 9 and 10;

Logarithmic regression equations;

$$E_{g\text{-}S} = -0.02\ln(d_t) + 0.319,\ R^2 = 0.969 \quad (9a)$$

$$E_{g\text{-}M} = -0.07\ln(d_t) + 0.957,\ R^2 = 0.969 \quad (9b)$$

Two-degree Polynomial regression equations;

$$E_{g\text{-}S} = 2\times10^{-5}\, d_t^2 - 0.002d_t + 0.281,\ R^2 = 0.988 \quad (10a)$$

$$E_{g\text{-}M} = 6\times10^{-5}\, d_t^2 - 0.006d_t + 0.845,\ R2 = 0.988 \quad (10b)$$

where d_t is the MWCNTs diameter. Eqs. 9 and 10 can be considered alternative expressions for Eqs. 2 and 3, respectively.

4. Conclusions

Multi-walled CNTs were synthesized from a $CaCO_3$-supported bimetallic (Fe-Ni) catalyst which was prepared by wet impregnation. Both the catalyst and the synthesized MWCNTs were characterized to investigate the suitability of the catalyst

and to study the effects of synthesis conditions on the CNTs properties. Peak shifts were observed in the XRD patterns of the nanotubes, suggesting crystal lattice deformations that could be responsible for variation in the energy gaps. The energy gaps of the MWCNTs (semi-conducting and metallic case) were obtained empirically from the TEM average diameter. Three different regression models were developed to analyze the effect of synthesis conditions on the Yield, Energy gap, and Aspect ratio of the nanotubes. These were used as the basis for a multiple response optimization that gave a global optimum. The regression models showed that the energy gap of the MWCNTs can be controlled by time, temperature, carrier gas, acetylene flowrate, and the interactions of (temperature-acetylene flowrate), and (time-temperature-acetylene flowrate). Also, the yield was affected by time, temperature, acetylene flowrate, and interactions of (time-acetylene flowrate), temperature-argon, and (temperature-acetylene flowrate); while the aspect ratio was influenced by temperature, argon flowrate, acetylene flowrate, and interaction of (temperature-argon flowrate). A Kataura plot for both the semi-conducting and metallic type MWCNTs was also made to establish empirical regression equations for both.

Conflict of Interest

No potential conflict of interest relevant to this article was reported.

Acknowledgements

Financial support received from Tertiary Education Trust Fund (TETFUND) Nigeria with grant number TETF/DESS/NRF/FUTM-2016/STI/1 is greatly appreciated. The authors are grateful to the Centre for Genetic Engineering and Biotechnology, Federal University of Technology, Minna for the assistance rendered during sample analysis. The authors wish to appreciate the following people that helped in analysing the samples: Dr Remy Bucher (XRD, ithemba Labs), Dr. Franscious Cummings (HRTEM, Physics department, University of the Western Cape (UWC), South Africa), Andrian Joseph (HRSEM, Physics department, UWC, South Africa).

References

[1] Abdulkareem AS, Kariim I, Bankole MT, Tijani JO, Abodunrin TF, Olu SC. Synthesis and characterization of tri-metallic Fe–Co–Ni catalyst supported on $CaCO_3$ for multi-walled carbon nanotubes growth via chemical vapor deposition technique. Arabian J Sci Eng, 42, 4365 (2017). https://doi.org/10.1007/s13369-017-2478-2.

[2] Bellucci S, Onorato P. Transport Properties in Carbon Nanotubes. In: Bellucci S, ed. Physical Properties of Ceramic and Carbon Nanoscale Structures. Lecture Notes in Nanoscale Science and Technology, Springer, Berlin, 45 (2011). https://doi.org/10.1007/978-3-642-15778-3_2.

[3] Prasek J, Drbohlavova J, Chomoucka J, Hubalek J, Jasek O, Adam V, Kizek R. Methods for carbon nanotubes synthesis: review. J Mater Chem, 21, 15872 (2011). https://doi.org/10.1039/c1jm12254a.

[4] Mohammed IA, Bankole MT, Abdulkareem AS, Ochigbo SS, Afolabi AS, Abubakre OK. Full factorial design approach to carbon nanotubes synthesis by CVD method in argon environment. S Afr J Chem Eng, 24, 17 (2017). https://doi.org/10.1016/j.sajce.2017.06.001.

[5] Mhlanga SD, Coville NJ. Iron-cobalt catalysts synthesized by a reverse micelle impregnation method for controlled growth of carbon nanotubes. Diamond Relat Mater, 17, 1489 (2008). https://doi.org/10.1016/j.diamond.2008.01.049.

[6] Liu C, Cheng HM. Carbon nanotubes: controlled growth and application. Mater Today, 16, 19 (2013). https://doi.org/10.1016/j.mattod.2013.01.019.

[7] Allaedini G, Tasirin SM, Aminayi P, Yaakob Z, Talib MZM. Bulk production of bamboo-shaped multi-walled carbon nanotubes via catalytic decomposition of methane over tri-metallic Ni–Co–Fe catalyst. React Kinet Mech Catal, 116, 385 (2015). https://doi.org/10.1007/s11144-015-0897-1.

[8] Duan X, Wang D, Qian G, Walmsley JC, Holmen A, Chen D, Zhou X. Fabrication of K-promoted iron/carbon nanotubes composite catalysts for the Fischer–Tropsch synthesis of lower olefins. J Energy Chem, 25, 311 (2016). https://doi.org/10.1016/j.jechem.2016.01.003.

[9] Abdalla S, Al-Marzouki F, Al-Ghamdi AA, Abdel-Daiem, A. different technical applications of carbon nanotubes. Nanoscale Res Lett, 10, 358 (2015). https://doi.org/10.1186/s11671-015-1056-3.

[10] Zaporotskova IV, Boroznina NP, Parkhomenko YN, Kozhitov LV. Carbon nanotubes: sensor properties. A review. Mod Electron Mater, 2, 95 (2016). https://doi.org/10.1016/j.moem.2017.02.002.

[11] Issi JP, Langer L, Heremans J, Olk CH. Electronic properties of carbon nanotubes: experimental results. Carbon, 33, 941 (1995). https://doi.org/10.1016/0008-6223(95)00023-7.

[12] Herranen O. Experimental Characterization of Electronic, Structural and Optical Properties of Individual Carbon Nanotubes, University of Jyväskylä, Jyväskylä, Finland, PhD Thesis (2014).

[13] Kharlamova MV, Volykhov AA, Yashina LV, Egorov AV, Lukashin AV. Experimental and theoretical studies on the electronic properties of praseodymium chloride-filled single-walled carbon nanotubes. J Mater Sci, 50, 5419 (2015). https://doi.org/10.1007/s10853-015-9086-x.

[14] Barone V, Scuseria GE. Theoretical study of the electronic properties of narrow single-walled carbon nanotubes: beyond the local density approximation. J Chem Phys, 121, 10376 (2004). https://doi.org/10.1063/1.1810132.

[15] Zhao J, Park H, Han J, Lu JP. Electronic properties of carbon nanotubes with covalent sidewall functionalization. J Phys Chem B, 108, 4227 (2004). https://doi.org/10.1021/jp036814u.

[16] Qiao W, Bai H, Zhu Y, Huang Y. Structure and electronic properties of the double-wall nanotubes constructed from SiO_2 nanotubes encapsulated inside zigzag carbon nanotubes. J Phys Condens Matter, 24, 185302 (2012). https://doi.org/10.1088/0953-8984/24/18/185302.

[17] Boutahir M, Rahmani AH, Fakrach B, Chadli H, Rahmani A. Theoretical study of electronic and vibrational properties of dimer of single-wall carbon nanotubes. Int J Hydrogen Energy, 41, 20874 (2016). https://doi.org/10.1016/j.ijhydene.2016.06.125.

[18] Yang N, Yang D, Chen L, Liu D, Cai M, Fan X. A first-principle theoretical study of mechanical and electronic properties in graphene single-walled carbon nanotube junctions. Materials, 10, 1300 (2017). https://doi.org/10.3390/ma10111300.

[19] Saito R, Dresselhaus G, Dresselhaus MS. Trigonal warping effect of carbon nanotubes. Phys Rev B, 61, 2981 (2000). https://doi.org/10.1103/physrevb.61.2981.
[20] Poncharal P, Berger C, Yi Y, Wang ZL, de Heer WA. Room temperature ballistic conduction in carbon nanotubes. J Phys Chem B, 106, 12104 (2002). https://doi.org/10.1021/jp021271u.
[21] Li HJ, Lu WG, Li JJ, Bai XD, Gu CZ. Multichannel ballistic transport in multiwall carbon nanotubes. Phys Rev Lett, 95, 086601 (2005). https://doi.org/10.1103/physrevlett.95.086601.
[22] Kataura H, Kumazawa Y, Maniwa Y, Umezu I, Suzuki S, Ohtsuka Y, Achiba Y. Optical properties of single-wall carbon nanotubes. Synth Met, 103, 2555 (1999). https://doi.org/10.1016/s0379-6779(98)00278-1.